# Kinetics of Cell Detachment: Peeling of Discrete Receptor Clusters

Michael D. Ward,* Micah Dembo,‡ and Daniel A. Hammer*
*School of Chemical Engineering, Cornell University, Ithaca, New York 14853, and ‡MS K-710, T10 Theoretical Biology, Los Alamos National Laboratory, Los Alamos, New Mexico 87545 USA

ABSTRACT Clustering of cell surface adhesion receptors is an essential step in the development of focal contacts, specialized cell-substrate attachment sites where receptors are simultaneously linked to extracellular ligand and cytoskeletal proteins. Previously, we examined the effect of receptor clustering on attachment strength. Here, we employ the numerical methodology developed by Dembo and colleagues (Dembo, M., D. C. Torney, K. Saxman, and D. Hammer. 1988. *Proc. R. Soc. Lond. B.* 234:55–83) to investigate the kinetics of cell detachment when receptors are clustered into discrete patches. We show that the membrane peeling velocity decreases if receptors are clustered within a patch located inside the contact region. Peeling of clusters is influenced by the chemistry and mechanics of receptor-ligand bonds within the patch. Detachment is also prohibited if the applied tension equals the critical tension of the patch, unless the patch length is small compared with the boundary length over which membrane bending occurs, in which case the patch will peel. Peeling of these short patches only occurs when the mechanical stiffness of clustered bonds is within an optimal range.

We compare our model predictions with experimental measurements of T lymphocyte detachment from ICAM-1 substrates. We demonstrate that if discrete patches of receptors are present, detachment occurs through intervals of slow and fast peeling, similar to the dynamics of T lymphocyte peeling, indicating that clustering of LFA-1 receptors is one possible explanation for the observed detachment kinetics in this system.

## INTRODUCTION

Many cell types possess surface adhesion receptors that bind selectively to extracellular ligand molecules. Receptor-ligand binding and the resulting adhesion influences cell growth (Ingber and Folkman, 1989; Ingber, 1990), differentiation (Ben-Ze'ev et al., 1988; Watt et al., 1988; Mooney et al., 1992), and motility (Couchman and Rees, 1979). During attachment and spreading, certain adhesion receptors associate with both ligand and cytoskeletal proteins in discrete sites of cell-substrate contact, known as focal contacts or focal adhesions, which contain many receptors and are tightly coupled (≤15 nm separation) to the substrate (Izzard and Lochner, 1976; Burridge et al., 1988; Dejana et al., 1988; Fath et al., 1989). The cytoskeleton likely strengthens the structural integrity of the focal adhesion, making the contact extremely resistant to removal forces (Rees et al., 1977). However, considerable increases in cellular adhesive strength may occur before complete cytoskeletally driven reinforcement of focal contacts as a result of receptor clustering, including within structures resembling precursor focal contacts (Lotz et al., 1989; Ward and Hammer, 1993). Focal adhesions are not the only physiologically important example of receptor clustering. Point contacts are patches of adhesion receptors that are much smaller than focal contacts (0.1–0.3 $\mu$m vs. 2–10 $\mu$m in length) and are rarely connected to actin filaments, yet contribute to attachment and spreading on ligand-coated substrates (Streeter and Rees, 1987; Tawil et al., 1993). To understand better how adhesion is regulated, it is therefore essential to examine the role of receptor clustering on cell-substrate adhesion and detachment.

Lotz et al. (1989) measured the relationship between the area of close (≤15 nm) cell-substrate contact—an index of cytoskeletal reorganization—and the attachment strength of glioma cells on fibronectin. Although glioma cells weakly bound the fibronectin substrate at 4°C, a dramatic (>10-fold) enhancement in adhesive strength occurred at 37°C. This strengthening response coincided with increased formation of ≤15 nm contacts and was abolished by addition of cytochalasin B, suggesting the involvement of cytoskeletal polymerization. When viewed under interference reflection microscopy, these ≤15 nm contacts did not resemble focal adhesions, but were more diffuse regions of close cell-substrate separation that only later developed into fully formed focal contacts. Adhesive strengthening may precede the appearance of focal contacts, because we found the reported increase in glioma cell adhesion strength could be attributed to cytoskeletally driven clustering of adhesion receptors, without the substantial enhancement in mechanical rigidity of the receptor-cytoskeleton cluster that likely accompanies focal contact maturation (Ward and Hammer, 1993).

Tözeren et al. (1992) used micropipet aspiration to measure the detachment of T lymphocytes from a planar membrane containing ICAM-1 ligand molecules. Although the LFA-1 receptor for ICAM-1 is constantly expressed on the lymphocyte surface, strong cell attachment to ICAM-1 was only observed after pretreatment of the T-cells with phorbol 12-myristate-13-acetate (PMA). Because previous studies demonstrated that LFA-1 associates with cytoskeletal proteins in PMA-treated cells but not in resting cells (Burn et al.,

*Received for publication 9 June 1993 and in final form 29 August 1994.*
Address reprint requests to Dr. Daniel A. Hammer, School of Chemical Engineering, Cornell University, 362 Olin Hall, Ithaca, NY 14853-5201. Tel.: 607-255-8681; Fax: 607-255-9166; E-mail: hammer @ cheme. cornell. edu.

0006-3495/94/12/2522/13 $2.00

1988), it is possible that the enhanced attachment strength of lymphocytes to ICAM-1 upon addition of PMA is a result of cytoskeletal cross-linking and clustering of LFA-1 receptors.

Several theoretical analyses have been developed to examine the influence of receptor and ligand chemistry on cell adhesion and spreading. Evans (1985a, b) solved the equations of mechanical equilibrium for a thin, inextensible membrane under the loading of continuous or discrete receptor-ligand cross-bridges. Because adhesion is treated as a purely conservative process in this model, the analysis is only valid at equilibrium; thus, Evans could derive the critical tension necessary to initiate membrane peeling, but could not compute the rate of peeling at tensions greater than critical because nonconservative dissipation was not included. To account for dissipation and to calculate the kinetics of peeling and spreading, Dembo and colleagues (1988) added strain-dependent rate constants for receptor-ligand binding onto the mechanical energy balances given by Evans. By including characteristic times for bond formation and breakage, which were related to the strain placed on individual cross-bridges, the rate of energy dissipation could be ascertained from the rate of bond deformation and dissociation, which in turn allowed calculation of the finite rate of membrane peeling (spreading) when the applied tension was greater (less) than the critical tension. Using this methodology, Dembo et al. (1988) determined how bond chemistry and bond mechanics influence the dynamics of cell spreading and detachment. Tözeren (1989) found that cell-cell detachment is restricted by accumulation of mobile receptor-ligand cross-bridges at the edge of contact during peeling, but he imposed a simple membrane geometry at the peeling edge, thereby neglecting membrane mechanics within the contact region. None of the above mechanical analyses considered the effect of discrete accumulations of receptors on the rate of peeling.

In an earlier paper, we examined how receptor clustering, driven by cytoskeletal cross-linking, affects cell-substrate attachment strength (Ward and Hammer, 1993). Because freely mobile adhesion receptors could simultaneously associate with cytoskeletal molecules (designated "talin") on cytoplasmic plaques and extracellular ligand, kinetic equations for the bond density resulting from receptor-ligand and receptor-talin binding were coupled to the equations of membrane mechanical equilibrium to calculate the critical tension when receptors were clustered on the cell surface. At high ligand and talin densities, extensive accumulation of adhesion receptors within the plaques resulted in a >10-fold enhancement in the adhesive strength over that obtained in the absence of receptor clustering. In fact, the quantitative match between our model and data on the strengthening response of glioma cell adhesion to fibronectin (Lotz et al., 1989) suggests that fibronectin induces receptor clustering in this cell type.

In the present work, we extend our earlier study to investigate the influence of receptor clustering on the dynamics of cell detachment from ligand-coated surfaces. Employing the methodology developed by Dembo et al. (1988), we calculate the rate of detachment of a membrane containing a patch of high receptor density. We find that peeling is inhibited by increased receptor clustering, whereas alterations in the chemical or mechanical properties of receptor-ligand bonds within the patch (compared with those outside the patch) can further strengthen the receptor cluster. In addition, we show that the tension required to peel the patch when the patch length is less than the membrane bending length is different than the critical tension, which corresponds to a membrane of infinite extent. Qualitative comparison of our model results with experimental measurements of T lymphocyte detachment from an ICAM-1-coated surface using micropipet aspiration (Tözeren et al., 1992) suggests that LFA-1 receptor clustering on the T lymphocyte surface is one possible explanation for the observed detachment kinetics.

## MATHEMATICAL MODEL

Fig. 1 illustrates the basic features of our one-dimensional tape-peeling model. The adhesive contact is divided into two regions: a) a microscopic region where receptor-ligand binding supports attachment and b) a macroscopic region where binding is negligible. At the outer edge of the macroscopic region, a tension $T_{mac}$ is applied at an angle $\theta_{mac}$ with the substrate. These calculations are performed under constant external load, $T_{mac}$. The membrane deflection is measured by the Cartesian coordinates $x$ and $y$, where $x$ is the horizontal distance along the surface and $y$ is the cell-substrate separation, as a function of membrane arclength, $s$.

Assuming quasi-mechanical equilibrium, a local balance of normal forces over the membrane gives (Evans and

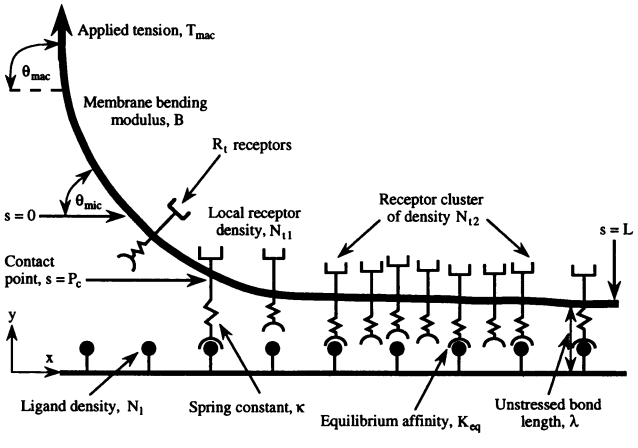


FIGURE 1 The geometry of the one-dimensional tape-peeling model is given by the coordinates $x$ and $y$ and the membrane arclength, $s$. In the macroscopic contact region ($s < 0$), binding is negligible and an applied tension, $T_{mac}$, acts at orientation $\theta_{mac}$, whereas in the microscopic region ($s \geq 0$), adhesive contact through receptor-ligand binding begins at the contact point, $s = P_c$. Cell surface receptors react with substrate ligand molecules to form spring-like bonds of mechanical stiffness $\kappa$ and length $\lambda$. In the model, receptors are clustered within discrete patches such that regions of low receptor density ($N_{t1}$) are adjacent to areas where the receptor density is substantially higher ($N_{t2}$).

Skalak, 1980; Evans, 1985a, b),

$$\frac{\partial}{\partial s}B\frac{\partial C}{\partial s} - CT = -\sigma_{nor}, \quad (1)$$

whereas the corresponding balance of tangential forces is

$$\frac{\partial T}{\partial s} + C\frac{\partial (BC)}{\partial s} = -\sigma_{tan}. \quad (2)$$

In these equations, $T$ is membrane tension, $C$ is membrane curvature, $B$ is the membrane bending modulus, and $\sigma_{nor}$ and $\sigma_{tan}$ are the normal and tangential components of the membrane stress, respectively. Following the framework of Dembo et al., (1988), we assume that the bending modulus is constant and that membrane stresses result from extension or compression of spring-like receptor-ligand bonds. In this case, $\sigma_{nor} = [N_b\kappa(y - \lambda)(\partial x/\partial s)]$ and $\sigma_{tan} = -[N_b\kappa(y - \lambda)(\partial y/\partial s)]$, where $\kappa$ measures the mechanical stiffness of the bond, $\lambda$ is the unstressed bond length, and $N_b$ is the local density of receptor-ligand bonds.

The arclength and curvature are related to the Cartesian coordinates,

$$\left(\frac{\partial x}{\partial s}\right)^2 + \left(\frac{\partial y}{\partial s}\right)^2 = 1 \quad (3)$$

and

$$C = \left(\frac{\partial x}{\partial s}\right)\left(\frac{\partial^2 y}{\partial s^2}\right) - \left(\frac{\partial^2 x}{\partial s^2}\right)\left(\frac{\partial y}{\partial s}\right). \quad (4)$$

Solution of Eqs. 1–4 using the appropriate boundary and matching conditions described in Appendix A yields the membrane morphology within the contact region.

The Peclet number, $L^2/t_pD$, where $L$ is the contact radius, $t_p$ is the time for peeling, and $D$ is the receptor diffusivity, measures the relative rates of receptor convection and diffusion during peeling. Because the Peclet number is typically O(100) (e.g., for $L \sim 5$ $\mu$m, $t_p \sim 30$ s, and $D \sim 10^{-10}$ cm$^2$ s$^{-1}$), receptor diffusion is minimal during detachment. (The receptors are "kinetically trapped," as Evans (1985b) first described.) Therefore, we assume that adhesion receptors are laterally fixed in position during peeling such that the total local density of receptors, $N_t$, is constant and equals $(N_f + N_b)$, where $N_f$ and $N_b$ are the local densities of free and ligand-bound receptors, respectively.

The density of receptor-ligand cross-bridges is given by a mass balance on bond density,

$$\frac{\partial N_b}{\partial t} = k_f(N_l - N_b)(N_t - N_b) - k_rN_b, \quad (5)$$

where $t$ is time, $k_f$ and $k_r$ are the forward and reverse binding rates, and $N_l$ is the ligand density. Because receptors are kinetically trapped, the density of adhesion receptors will remain uniform during peeling, $\partial N_t/\partial t = 0$.

At the edge of molecular contact between cell and substrate, defined by the contact point, $s = P_c$, the bond density equals a critically low value $N_{bc}$, ensuring that binding stresses are negligible at values of $s$ below this point. The velocity at which the contact radius decreases during detachment, $V_p$, is given by $V_p = \partial P_c/\partial t$ (Dembo et al., 1988). Changing to a cell reference frame fixed at the contact point, $\tilde{s} = s - P_c$, introduces an apparent convective term in the mass balance equation,

$$\frac{\partial N_b}{\partial t} = V_p\frac{\partial N_b}{\partial \tilde{s}} + k_f(N_l - N_b)(N_t - N_b) - k_rN_b. \quad (6)$$

The first term on the right hand side of (6) does not represent a true membrane convection, but rather a co-moving derivative contribution caused by the moving reference frame. Because $N_b$ always equals $N_{bc}$ at $\tilde{s} = 0$, the peeling velocity is explicitly given by

$$V_p = \left\{-[k_f(N_l - N_b)(N_t - N_b) - k_rN_b]\Big/\frac{\partial N_b}{\partial s}\right\}\Bigg|_{\tilde{s}=0} \quad (7)$$

For spring-like receptor-ligand bonds, the rate constants for binding are functions of cell-substrate separation (Dembo et al., 1988; Hammer and Apte, 1992),

$$k_f = k_{feq}\exp\{-\kappa_{ts}(y - \lambda)^2/2k_b\Theta\} \quad (8)$$

and

$$k_r = k_{req}\exp\{(\kappa - \kappa_{ts})(y - \lambda)^2/2k_b\Theta\}, \quad (9)$$

where $k_{feq}$ and $k_{req}$ are the rate constants for unstressed bonds, $\kappa_{ts}$ is the transition state spring constant, and $k_b\Theta$ is the thermal energy. The affinity between receptor and ligand, $K$, is

$$K = k_f/k_r = K_{eq}\exp\{-\kappa(y - \lambda)^2/2k_b\Theta\}, \quad (10)$$

where $K_{eq}$ is the equilibrium affinity for an unstressed bond.

When $\kappa_{ts} = \kappa$, bonds break at the same rate irrespective of bond strain $(y - \lambda)$. For $\kappa_{ts} < \kappa$, bond rupture increases with strain, whereas in the "catch"-state ($\kappa_{ts} > \kappa$), unstressed bonds actually dissociate faster than extended or compressed cross-bridges. Because catch-bonds do not permit detachment (Dembo et al., 1988), we only consider slip-bonds ($\kappa_{ts} \leq \kappa$) in this analysis.

The center of contact is substantially far inside the peeling edge such that the membrane remains firmly clamped to the substrate at a separation equal to the unstressed bond length at $s = L$ (see Appendix A). Therefore, the bond density at this point is unaffected by peeling ($\partial N_b/\partial s = 0$) and, at steady state ($\partial N_b/\partial t = 0$), one can define an equilibrium bond density, $N_{beq}$, from solution of a modified form of Eq. 6, $0 = K_{eq}(N_l - N_{beq})(N_t - N_{beq}) - N_{beq}$.

In our earlier model for the role of focal contact formation on adhesion strength, the cross-linking and clustering of adhesion receptors by cytoskeletal proteins resulted in greater densities of receptor molecules associated with cytoskeleton plaques (Ward and Hammer, 1993). Therefore, to measure rates of peeling when receptors are clustered within patches, we assume that there are discrete regions of the cell surface where the receptor density, $N_{t2}$, is much larger than that found

in areas outside the patches, $N_{t1}$. We assume that patches occupy 10% of the total contact area, consistent with estimates of the total area of focal contacts (Ward and Hammer, 1993). Defining $f_{Nt} = N_{t2}/N_{t1}$, the density of receptors outside patches is obtained from a balance on receptors,

$$N_{t1} = R_t/[\pi L^2(0.9 + 0.1f_{Nt})], \quad (11)$$

whereas the receptor density within patches is $N_{t2} = f_{Nt}N_{t1}$.

In cell reference frame coordinates ($\tilde{s} = s - P_c$), the time-dependent binding equation is given by Eq. 6, with the additional constraint that the total receptor density equation is similarly transformed to account for the co-moving derivative contribution to motion of the adhesive patch,

$$\frac{\partial N_t}{\partial t} = V_p \frac{\partial N_t}{\partial \tilde{s}}. \quad (12)$$

For patch peeling, $V_p$ is calculated from Eq. 7 and used in conjunction with Eq. 12 to update the location of the patch. Furthermore, two forms of Eq. 6 are required for inside and outside the patch.

During clustering, it is possible that the chemical or mechanical properties of adhesion receptors within the patch are modulated by association with the cytoskeleton. We distinguish between the affinity, mechanical stiffness, and reactive compliance for receptors that are ($i = 2$) or are not ($i = 1$) clustered using different subscripts.

## Critical Tension

The critical tension, $T_{crit}$, is the minimum applied tension that exactly balances adhesion forces ($V_p = 0$). Tensions above this critical value induce cell detachment ($V_p > 0$); tensions below induce spreading ($V_p < 0$). In this paper, we use the term critical tension to indicate the tension required to peel a membrane of infinite extent, so that we can distinguish the response of finite patches from infinite stretches of membrane. Therefore, it will be possible for a finite membrane patch to peel at tensions below the critical tension. We follow the procedure of Dembo et al. (1988) to determine $T_{crit}$ (Dembo et al., 1988; Ward and Hammer, 1993). To calculate critical tensions corresponding to the mass balance described by Eq. 6, which permits the depletion of ligand, we had to extend the results presented originally by Dembo et al. (1988), who restricted their attention to the excess ligand limit. A complete description of how the ligand density affects the critical tension will be published elsewhere (Hammer et al., 1994).

## Model Analysis

The scaling analysis, nondimensional equations, and finite difference algorithm used to solve Eqs. 1–4, 6–10, and 12 are presented in Appendix A. In Table 1, we list the important dimensional parameters involved in our model and present ranges of these parameters based upon theoretical estimates or independent experimental measurements. Dimensionless groups are shown in Table 2. $f_{Nt}$ is the index of the amount of receptor clustering within patches. Because receptor clustering through cytoskeletal cross-linking may alter receptor properties, we examine the peeling dynamics when receptors inside the patch bind ligand with higher affinity ($\omega_2 > \omega_1$) or form bonds that have smaller reactive compliances ($f_{\kappa 2} < f_{\kappa 1}$) or have greater mechanical stiffness ($\phi_2 > \phi_1$) from those outside the patch.

## RESULTS

In Fig. 2, we plot the dimensionless peeling velocity, $\bar{V}_p$, as a function of dimensionless time, $\bar{t}$, for different values of $\bar{T}_{mp}$, the applied tension scaled to the critical tension calculated based on the density in the patch. In this calculation, the patch length ($\delta_p$) is greater than the length over which membrane bending occurs (Evans, 1985a). For all values of $\bar{T}_{mp}$, an initial steady-state velocity is reached that corresponds to peeling of the membrane region outside the patch. Because peeling slows as $\bar{T}_{mp}$ decreases, the patch reaches the contact point at longer times for lower $\bar{T}_{mp}$ ($\bar{t} \approx 75$ when $\bar{T}_{mp} = 0.5$ vs. $\bar{t} \approx 35$ when $\bar{T}_{mp} = 2$). The adhesive patch inhibits membrane peeling, because $\bar{V}_p$ is substantially reduced as the patch nears the contact point. If $\bar{T}_{mp} > 1$, membrane peeling proceeds, albeit at a slower rate. In this case, $\bar{V}_p$ displays interesting dynamic behavior, including an overshoot, an undershoot, and damped oscillations as the steady-state velocity of the patch is reached. Although the initial overshoot (occurring for $\bar{t} \leq 10$) is likely an artifact caused by the numerical algorithm and idealized initial state of the membrane, the dynamic behavior displayed as the edge of contact

**TABLE 1 Estimates for dimensional parameters of the model**

| Parameter | Definition | Physiological range | Source |
|---|---|---|---|
| $A_{cell}$ | Cell area | $10^2$–$10^4$ $\mu m^2$ | Bell et al. (1984) |
| $B$ | Bending modulus | 0.4–4 $\times$ $10^{-12}$ ergs | Evans (1983); Engelhardt et al. (1985); Duwe et al. (1990) |
| $k_b\Theta$ | Thermal energy | 3.8–4.3 $\times$ $10^{-14}$ ergs | |
| $k_r$ | Reverse reaction rate | $10^{-5}$–$10^1$ $s^{-1}$ | Pecht and Lancet (1977); Bell (1978) |
| $K_{eq}$ | Receptor-ligand affinity | $10^{-10}$–$10^{-5}$ $cm^2$ | Bell et al. (1984); Dembo et al. (1988) |
| $L$ | Contact radius | 5–30 $\mu m$ | Bell et al. (1984) |
| $L_p$ | Patch length | <0.1–10 $\mu m$ | Izzard and Lochner (1976); Streeter and Rees (1987); Tawil et al. (1993) |
| $N_l$ | Ligand density | $10^6$–$10^{12}$ $cm^{-2}$ | Massia and Hubbell (1991) |
| $R_t$ | Receptor number | $10^4$–$10^6$ | Bell et al. (1984); Akiyama et al. (1990) |
| $\lambda$ | Receptor-ligand bond length | 10–100 nm | Bell et al. (1984) |
| $\kappa$, $\kappa_{ts}$ | Spring constant | $10^{-2}$–$10^1$ dyn $cm^{-1}$ | Bell et al. (1984); Dembo et al. (1988) |

**TABLE 2 Dimensionless parameters**

| Symbol* | Expression | Definition |
|---|---|---|
| $\alpha$ | $2\pi L^2/A_{cell}$ | Dimensionless contact area |
| $\beta_i$ | $\kappa_i\lambda^2/2k_b\Theta$ | Bond energy/thermal energy |
| $\delta$ | $\lambda/L$ | Bond length/contact area radius |
| $\delta_p$ | $L_p/L$ | Patch length/contact area radius |
| $\epsilon$ | $N_t A_{cell}/R_t$ | Ligand density/receptor density |
| $\zeta$ | $R_t L^2/A_{cell}$ | Dimensionless receptor density |
| $\phi_i$ | $\kappa_i L^2/B$ | Bond energy/bending energy |
| $\omega_i$ | $K_{eqi}R_t/A_{cell}$ | Dimensionless receptor-ligand affinity |
| $f_{\kappa i}$ | $(\kappa_i - \kappa_{tsi})/\kappa_i$ | Reactive compliance |
| $f_{Nt}$ | $N_{t2}/N_{t1}$ | Clustering factor |
| $N_{bcrit}$ | $N_{bc}/N_{beql}$ | Critical bond density |

* The subscript $i$ denotes the properties of receptors outside ($i = 1$) or inside ($i = 2$) the receptor cluster.

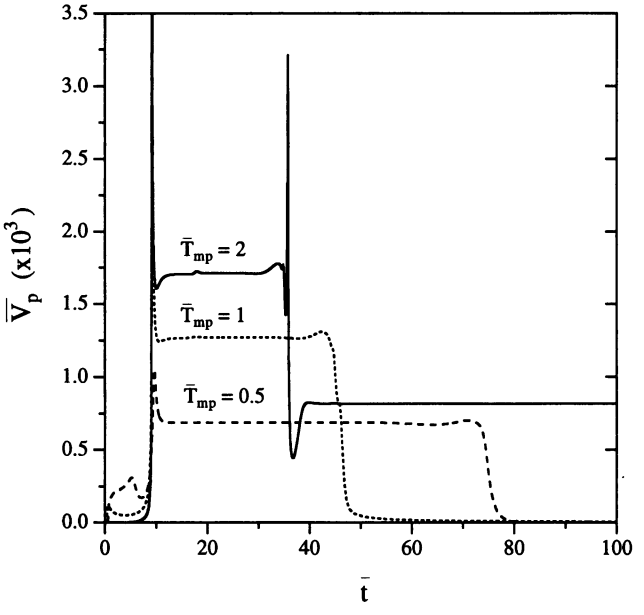


FIGURE 2 The time dependence of the dimensionless peeling velocity, $\bar{V}_p$, when a patch of high receptor density is located just inside the contact point is examined for three values of $\bar{T}_{mp}$, the ratio of the applied tension scaled to the critical tension of the patch. The patch is substantially longer than the length over which membrane bending occurs (Evans, 1985a). Parameter values are $\alpha = 0.628$, $\beta_1 = \beta_2 = 48.8$, $\delta = 2 \times 10^{-3}$, $\delta_p = 0.2$, $\epsilon = 1$, $\zeta = 10^4$, $\phi_1 = \phi_2 = 10^6$, $\omega_1 = \omega_2 = 1$, $f_{\kappa 1} = f_{\kappa 2} = 0$, $f_{Nt} = 10$, and $N_{bcrit} = 10^{-4}$. The patch is initially located at the dimensionless arclength $\bar{s} = P_{beg} = 0.05$.

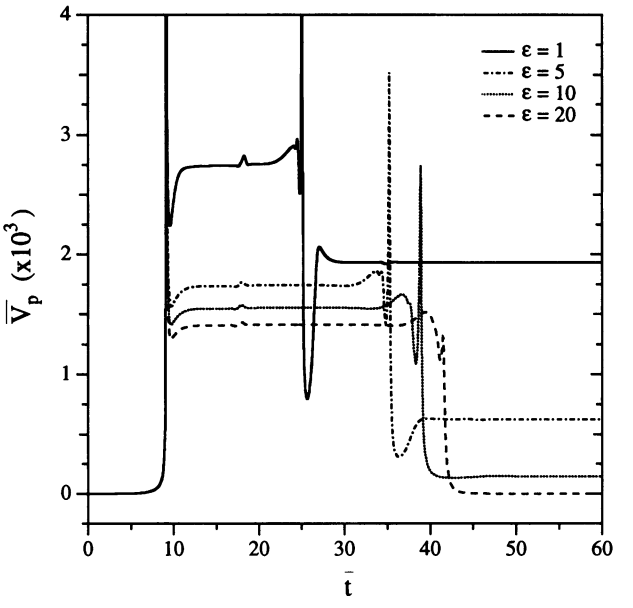


FIGURE 3 Effect of the dimensional ligand density, $\epsilon$, on the peeling velocity, $\bar{V}_p$. Parameter values are identical to Fig. 2 except that $T_{mac} = 0.012$ dyn cm$^{-1}$.

moves into the patch is more likely observable. The patch does not peel ($\bar{V}_p = 0$) if $\bar{T}_{mp} \leq 1$.

When adhesion occurs in the presence of cytoskeletal plaques that are capable of cross-linking adhesion receptors, increases in ligand density promote receptor clustering within these plaques compared with other regions of the cell surface (see Fig. 6 *A* in Ward and Hammer, 1993). To establish the effect of ligand density on the peeling of receptor clusters, we show how $\bar{V}_p$ depends on dimensionless ligand density, $\epsilon$, for a fixed applied tension (0.012 dyn cm$^{-1}$) (Fig. 3). Because $f_{Nt}$ is constant, changes in $\epsilon$ do not alter the number of receptors located either inside or outside the patch. However, the fraction of these receptors bound to ligand increases as $\epsilon$ increases, resulting in diminished rates of membrane peeling at high $\epsilon$. For $\epsilon = 1$, $\bar{V}_{pss} \approx 2.75 \times 10^{-3}$ and $\bar{V}_{pss} \approx 1.9 \times 10^{-3}$ when peeling non-patch and patch regions, respectively. Both velocities decrease as $\epsilon$ is increased, until a critical ligand density ($\epsilon = 20$) is reached, at which point $\bar{V}_{pss} = 0$ for the patch; hence, detachment of the patch is prohibited. Note also that larger oscillations in $\bar{V}_p$ occur at low $\epsilon$.

We examine the effect of $f_{Nt}$ on $\bar{V}_p$ when $\epsilon$ is high in Fig. 4. The ligand density is constant in this case, but greater clustering (increased $f_{Nt}$) results in the accumulation of receptors within the patch at the expense of non-patch regions. When $f_{Nt} = 1$, the receptor density is uniform throughout the cell-substrate contact and the membrane peels at a single steady-state rate, $\bar{V}_{pss} \approx 1.2 \times 10^{-3}$ (Fig. 4 *a*). A 10-fold clustering ($f_{Nt} = 10$) leads to a similar factor of decline in the peeling rate of the patch ($\bar{V}_{pss} \approx 1.2 \times 10^{-4}$), whereas modestly increasing the peeling velocity of regions outside the patch ($\bar{V}_{pss} \approx 1.7 \times 10^{-3}$). Integrating $\bar{V}_p(\bar{t})$ over time, we calculate the fraction of the entire adhesive contact remaining attached to the substrate, $\bar{L}_c$, as a function of the dimensionless time (Fig. 4 *b*). After an initial lag phase, $\bar{L}_c$ decreases rapidly until the patch is reached, at which point peeling slows. The initial drop in $\bar{L}_c$, corresponding to peeling of regions outside the adhesive patch, is most severe at high $f_{Nt}$ because $\bar{V}_{pss}$ of non-patch regions is greatest when $f_{Nt}$ is large. However, because $\bar{V}_{pss}$ of the patch is substantially reduced as clustering ($f_{Nt}$) increases, peeling of the entire interface will require much longer times when $f_{Nt}$ is high. For example, although cell detachment ($\bar{L}_c = 0$) occurs at $\bar{t} \approx 840$ for $f_{Nt} = 1$, the patch $\bar{V}_{pss}$ equals zero when $f_{Nt} = 20$, such that membrane peeling stops when $\bar{L}_c = 0.95$ (i.e., $\bar{t}$ for peeling is infinite).

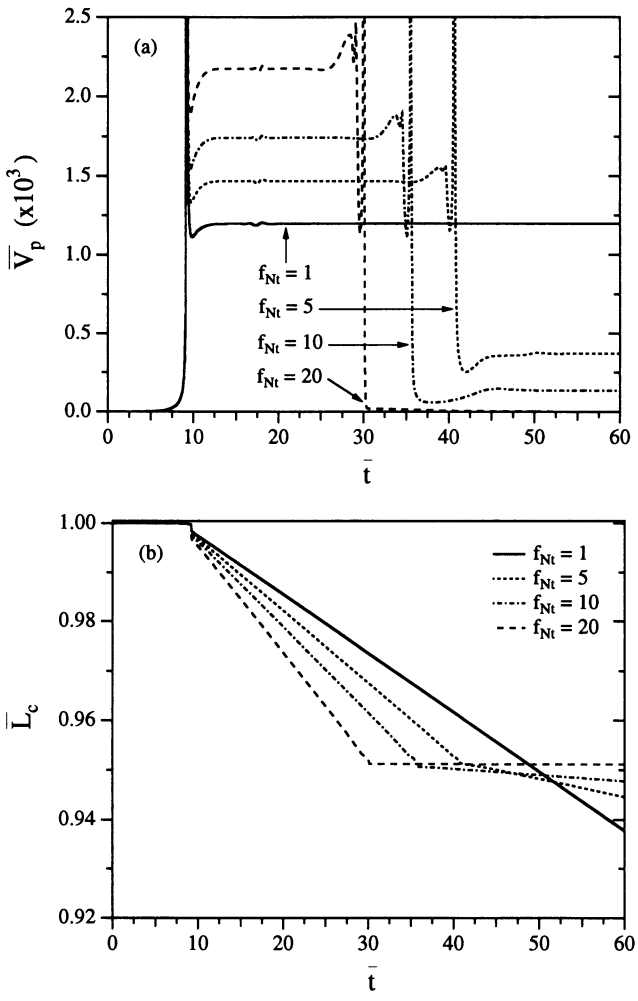


FIGURE 4 Effect of clustering factor, $f_{Nt}$, on membrane peeling. (*a*) $\bar{V}_p$, as a function of dimensionless time. (*b*) Dimensionless contact radius, $\bar{L}_c$, as a function of dimensionless time. The parameter values are the same as Fig. 2, except that $\epsilon = 20$ and $T_{mac} = 0.02$ dyn cm$^{-1}$.

Figs. 3 and 4 demonstrate that cell detachment is delayed, or even prevented, when receptor clusters are present. Although changes in ligand density ($\epsilon$) or the clustering index ($f_{Nt}$) affect the density of receptor-ligand bonds within patches, which consequently influences the attachment strength and detachment dynamics of the membrane, peeling of an adhesive patch may be altered by modulation of the chemical or mechanical properties of individual bonds within the patch when the level of receptor clustering remains constant. For example, biochemical modification of adhesion receptors after cytoskeletally driven clustering may enhance the affinity between receptor and ligand, or strengthen receptor-ligand bonds, thereby enabling the bonds to withstand greater levels of strain before rupturing. Therefore, we examine how changes in the affinity ($\omega_2$) and reactive compliance ($f_{\kappa 2}$) of bonds within the patch affect membrane peeling when the properties of receptor-ligand bonds outside the patch ($\omega_1$ and $f_{\kappa 1}$) remain fixed.

When the receptor-ligand affinity for bonds outside the patch, $\omega_1$, is constant, changes in the affinity, $\omega_2$, between ligand and clustered bonds do not change the peeling velocity, $\bar{V}_p$, of non-patch regions (Fig. 5, $\bar{t} < 25$). Increases in $\omega_2$ reduce the steady-state peeling velocity of the patch, although considerable (100-fold) enhancements give only a slight (< twofold) decrease in $\bar{V}_{pss}$. The weak dependence of $\bar{V}_{pss}$ on affinity is because the maximum bond density within the patch is limited by available ligand ($\epsilon = 1$) in this case. Thus, although a 10-fold increase in ligand density proportionally reduces $\bar{V}_{pss}$ of the patch (Fig. 3), large changes in $\omega_2$ have a minor influence on membrane peeling in this regime.

Fig. 6 shows the peeling velocity, $\bar{V}_p$, as the reactive compliance of bonds inside the patch ($f_{\kappa 2}$) is varied for a fixed reactive compliance of non-patch bonds ($f_{\kappa 1}$). Variation in the reactive compliance, keeping all other dimensionless parameters fixed, is tantamount to varying $\kappa_{tsi}$, which has the additional effect of altering the forward reaction rate. Nevertheless, increasing $f_{\kappa 2}$ has the effect of increasing the rate of breakage under a fixed strain. Increases in the strength of patch bonds (decreasing $f_{\kappa 2}$) lead to slower rates of membrane peeling (lower $\bar{V}_p$) and significantly affect the transient behavior of $\bar{V}_p$ as the patch approaches the edge of contact. Because changes in reactive compliance alter the peeling velocity without influencing the critical tension (Dembo et al., 1988), membrane peeling is always possible ($\bar{V}_{pss} > 0$) for this level of applied tension ($\bar{T}_{mp} = 2$) provided $f_{\kappa 2} \geq 0$. Catch-bonds ($f_\kappa < 0$) prevent peeling even when the applied tension exceeds the critical tension (Dembo et al., 1988), suggesting that biochemical modifications of clustered receptor-ligand cross-bridges that reduce $f_{\kappa 2}$ toward the catch-state will substantially inhibit cell detachment.

In previous figures, the ability to reach an asymptotic peeling velocity is a function of the size of the patch compared with the length of a boundary region, $\tau$, which depends in-

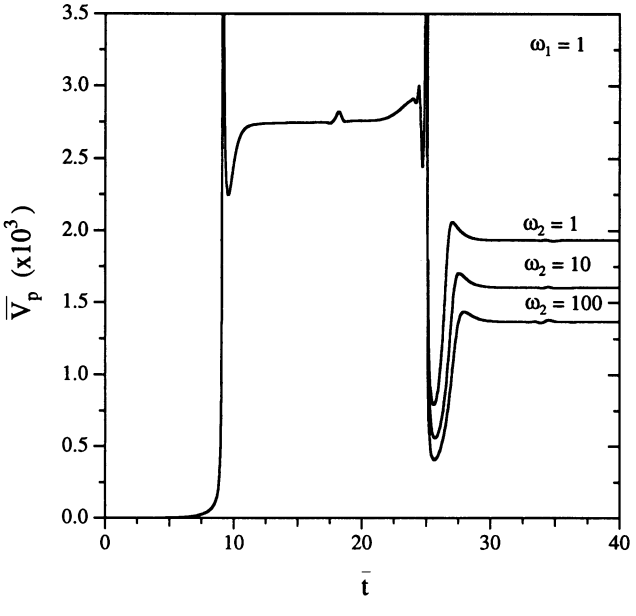


FIGURE 5 Effect of affinity of receptors in the patch, $\omega_2$, on peeling velocity $\bar{V}_p$. Parameter values are given in Fig. 2, except that $T_{mac} = 0.012$ dyn cm$^{-1}$.

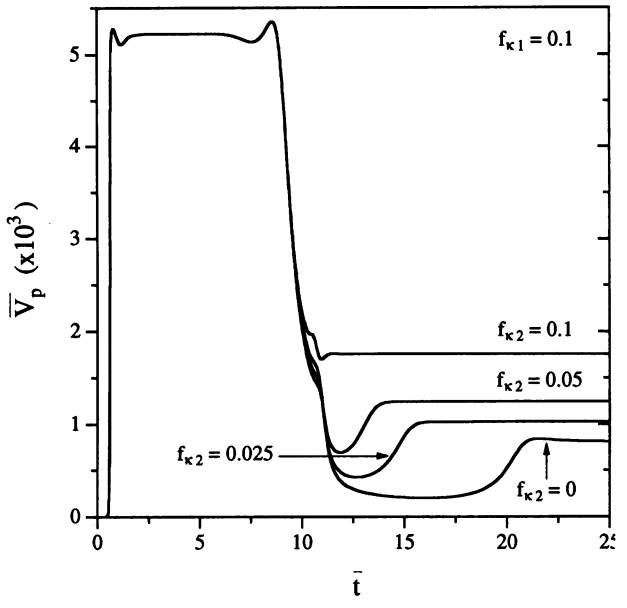


FIGURE 6 Peeling velocity, $\bar{V}_p$, as a function of the reactive compliance of bonds located inside the patch, $f_{\kappa 2}$, with the reactive compliance of bonds outside the patch fixed at $f_{\kappa 1} = 0.1$. The parameters are the same as Fig. 2 except $\bar{T}_{mp} = 2$.

versely on the adhesive energy in the patch (Evans, 1985). $\bar{V}_{pss}$ for the patch exists when $\delta_p \gg \tau$. Conversely, if the patch length is comparable with, or less than, the boundary length, it is not clear whether one will observe steady-state peeling of the patch and, consequently, whether a steady-state velocity can be defined. We have performed calculations for different patch sizes to show that, depending on the properties of the molecules in the patch, small patches will peel, even if $\bar{V}_{pss}$ for a larger patch of equivalent bond density is zero (data not shown).

We also explore whether biochemically induced changes in the mechanical stiffness ($\phi_2$) of adhesive cross-bridges within a patch of length $\delta_p = 0.005$ affect the dynamics of peeling (Fig. 7). Strictly, $\phi_2$ is the ratio of the mechanical stiffness of the molecules compared with the bending rigidity. We performed these calculations keeping the ratio $\phi_2/\beta_2$ and $f_{\kappa 2}$ constant. Therefore, increases in $\phi_2$ can be thought of as increases in the bond stiffness or decreases in the bending rigidity of the membrane, with concomitant changes in $\kappa_{tsi}$ to keep the reactive compliance constant. We refer to $\phi_2$, as it

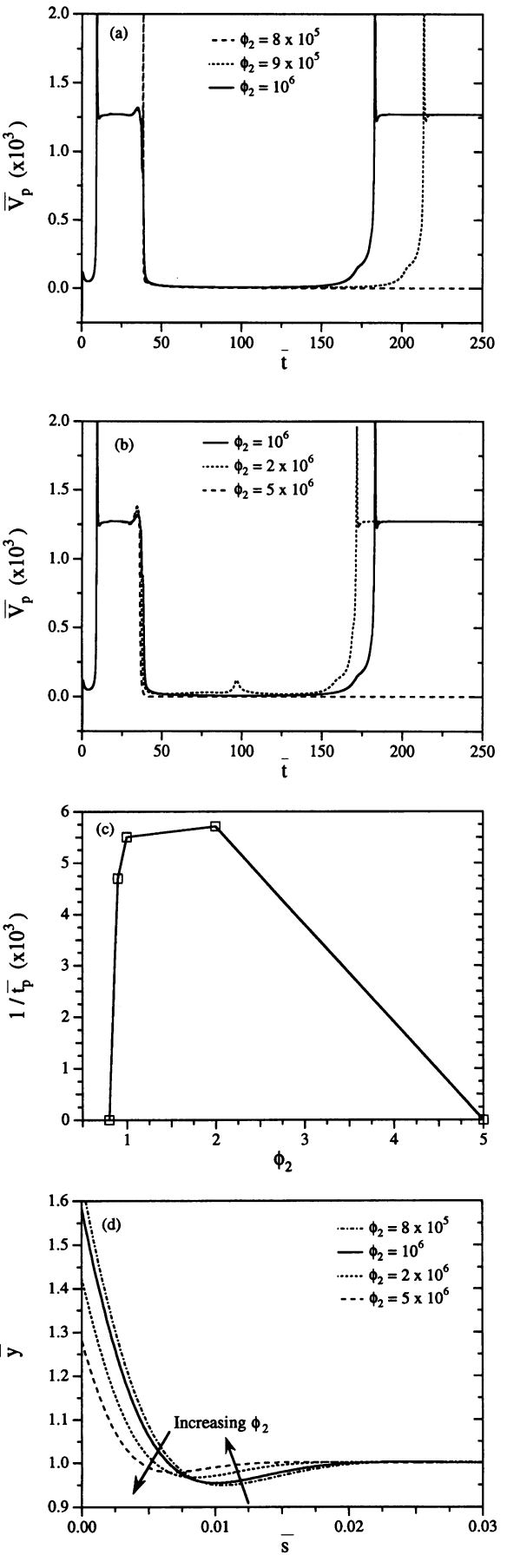


FIGURE 7 The effect of ratio of the mechanical stiffness the membrane bending rigidity, $\phi_2$, of clustered receptor-ligand bonds on the detachment dynamics when the patch length, $\delta_p$, is less than $\tau$, the boundary length for membrane bending. The patch is completely peeled by the dimensionless time, $\bar{t} \approx 180$, when $\phi_2 = 10^6$. (*a*) Although a small decrease in $\phi_2$ ($9 \times 10^5$) extends the time necessary to peel the patch ($\bar{t} \approx 215$), the patch will not peel ($\bar{V}_p = 0$) if $\phi_2$ is further reduced to $8 \times 10^5$. (*b*) Slightly stiffer bonds ($\phi_2 = 2 \times 10^6$) support faster peeling. Peeling of the patch is prohibited if the bonds are too rigid ($\phi_2 = 5 \times 10^6$). (*c*) Effect of the $\phi_2$ on the rate of peeling. (*d*) Effect of $\phi_2$ on the shape of the membrane. The parameters used in these calculations are the same as in Fig. 2 except, that $\delta_p = 5 \times 10^{-3}$ and $\phi_2/\beta_2 = 2.05 \times 10^4$.

is altered in these simulations, as the bond stiffness. When $\phi_2 = 10^6$, the patch peels even though $\bar{T}_{mp} = 1$ because the patch length, $\delta_p$, is much smaller than the boundary length, $\tau$, over which membrane bending is observed. In this case, the time, $\bar{t}_p$, to completely peel the patch is ≈180. Fig. 7 *a* reveals that although small decreases in the relative bond stiffness ($\phi_2 = 9 \times 10^5$) delay the peeling of the patch ($\bar{t}_p \approx 215$), peeling is completely abolished if the relative stiffness is too small ($\bar{t}_p \to \infty$ when $\phi_2 = 8 \times 10^5$). Faster peeling is observed when bond stiffness is increased ($\phi_2 = 2 \times 10^6$). However, when the stiffness is further increased ($\phi_2 = 5 \times 10^6$), peeling is once again prevented (Fig. 7 *b*). Thus, detachment of a patch of length $\delta_p$ when $\delta_p < \tau$ occurs in a finite time ($1/\bar{t}_p > 0$) only when the spring constant is within an intermediate range (Fig. 7 *c*); when $\phi_2$ is too low or too high, membrane peeling is prohibited. This dependence of $\bar{t}_p$ on $\phi_2$ cannot be explained by changes in the critical tension, $T_{crit}$, of the equivalent infinite patch because changes in the spring constant do not alter $T_{crit}$ (Dembo et al., 1988). Rather, increasing $\phi_2$ has two opposing effects: a) to increase the peeling velocity (Dembo et al., 1988) and b) decrease the boundary length (Fig. 7 *d*) (Evans, 1985a). When $\phi_2 = 10^6$, $\delta_p < \tau$ and the patch peels. $\bar{V}_p$ of the patch increases slightly when $\phi_2$ is raised to $2 \times 10^6$ and, because $\tau$ is still $> \delta_p$, peeling of the patch requires less time. One would expect $\bar{t}_p$ to be even smaller when $\phi_2 = 5 \times 10^6$ because of the dependence of $\bar{V}_p$ on the spring constant. However, the bending length decreases ($\tau = \delta_p$ in this case) and the patch peels as if it is infinite; because $\bar{T}_{mp} = 1$, $\bar{V}_p = 0$. Although the boundary length changes slightly when $\phi_2 < 10^6$, the reduction in the peeling velocity of the patch with decreasing $\phi_2$ is the major reason why $\bar{t}_p$ increases in these instances. Thus, biochemical modulation of the mechanical stiffness of receptor-ligand bonds within small clusters can dramatically alter detachment kinetics.

## COMPARISON WITH EXPERIMENT

The results of this paper indicate how receptor and ligand chemistry and the clustering of adhesion receptors influence the strength of cell-substrate attachment and alter the dynamics of cell detachment. In this section, we discuss experimental methods that may permit verification of specific model predictions, and qualitatively examine measurements of the kinetics of T lymphocyte detachment from an ICAM-1 surface (Tözeren et al., 1992).

It is possible to produce substrates of different ligand density (Cozens-Roberts et al., 1990; Massia and Hubbell, 1990). Also, cell lines expressing altered fibronectin receptors are available; these receptors bind ligand but do not associate with the cytoskeleton (Marcantonio et al., 1990; Reszka et al., 1992). These cell lines should show altered patterns of receptor clustering that may facilitate the observation of detachment dynamics as a function of receptor clustering. Finally, because micropipet aspiration allows one to measure the membrane tension during detachment, the total contact area, and the cell-substrate contact angle, it should prove possible to test model predictions concerning the influence of ligand density, receptor number, and receptor-ligand affinity on the critical tension and peeling velocity.

To evaluate quantitatively the influence of receptor clustering on the dynamics of cell detachment, one must first identify whether receptor aggregates form after initial attachment and ascertain the location and size of these patches. Although immunofluorescent labeling of adhesion receptors has been successfully implemented to discern clusters of adhesion receptors (Dejana et al., 1988; Fath et al., 1989), no one has simultaneously observed receptor clustering and measured detachment kinetics because concurrent micropipet aspiration and cluster identification requires observation angles that are perpendicular to each other, and therefore involves complicated design considerations. Although quantitative evaluation of our model is not possible in the absence of such experiments, we utilize our theoretical framework to determine whether receptor clustering can explain recent measurements of the detachment kinetics of T lymphocytes from ICAM-1 substrates (Tözeren et al., 1992).

Because an integral component of T lymphocyte adhesion to a variety of cell types is the association of the LFA-1 receptor on the T-cell with its counterreceptor, ICAM-1 (Springer, 1990), Tözeren et al. (1992) measured detachment of PMA-treated T lymphocytes from a planar layer of ICAM-1 molecules using micropipet aspiration (Fig. 8). For all cells studied, cell detachment occurred in two distinct stages: a) a gradual reduction of the contact radius initially, followed by b) substantially higher peeling rates that continued until detachment was complete. However, the behavior of individual cells was significantly different. For example, in one instance (Fig. 8, *circles*) detachment proceeded through "stop-and-go" peeling—intervals of fast peeling surrounding a period of extremely slow detachment. Because LFA-1 receptors on PMA-stimulated lymphocytes associate

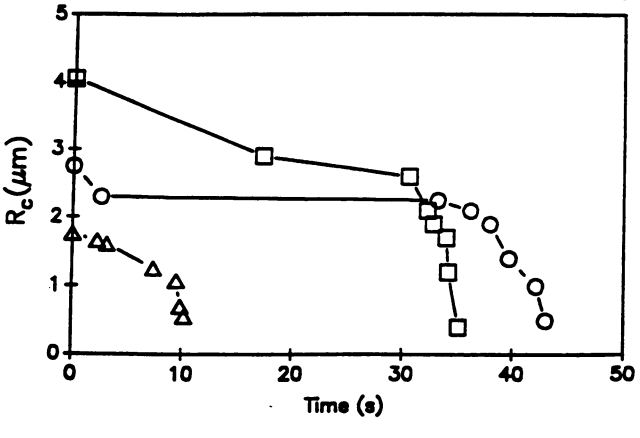


FIGURE 8 The time-dependent decrease in the contact radius during micropipet aspiration of T lymphocytes from an ICAM-1 substrate (Tozeren et al., 1992). In each of the three experiments shown in this plot, detachment progresses from an initial slow peeling to a more rapid reduction in the contact radius until detachment is complete. Reproduced from the *Biophysical Journal*, 1992, Vol. 63, 247–258, by copyright permission of the Biophysical Society.

with the cytoskeletal protein talin (Burn et al., 1988), a component of focal contacts in fibroblasts and other cell types, it is quite possible that LFA-1 receptors were clustered on the lymphocyte surface through cross-linking by talin. We therefore examine whether the observed detachment behavior of T lymphocytes on ICAM-1 substrates can be explained by the presence of discrete patches of LFA-1 receptors.

Because of the absence of information on the presence, size, and location of LFA-1 clusters, rigorous quantitative comparison between model and experiment is impossible. However, many of the model parameters were measured, or can be estimated, for the LFA-1/ICAM-1 system, which allows us to improve significantly the accuracy of a qualitative comparison. For example, lymphocytes possess a surface area of approximately $2 \times 10^{-6}$ cm$^2$ (Roitt et al., 1989) and typically express $10^5$ LFA-1 receptors (Sung et al., 1992). In the detachment experiments performed by Tözeren et al. (1992), the time-dependent decrease in contact radius was directly measured while the ICAM-1 density was fixed at $10^{11}$ cm$^{-2}$. Additionally, as an estimate, if Young's equation is valid in these experiments, the reported adhesive energies and contact angles for T lymphocyte attachment to ICAM-1 substrates suggests that the macroscopic applied tension is $\approx$0.1 dyn cm$^{-1}$.

In Fig. 9, we present model results for the detachment kinetics of T lymphocytes from an ICAM-1 substrate. We assume that LFA-1 receptors are clustered within an adhesive patch located interior ($\bar{s} = 0.3$) to the contact point. We then determine the rate at which the dimensionless contact radius ($\bar{L}_c$) decreases as the amount of clustering, the patch size, and the chemical or mechanical properties of clustered bonds is varied. Although detachment is complete when $\bar{L}_c = 0$, we do not extend our calculations below $\bar{L}_c = 0.2$ because the center of contact ($s = L$) can no longer be considered a clamped extremity at this value of $\bar{L}_c$ (Appendix A).

Surprisingly, we find that greater clustering (higher $f_{Nt}$) of LFA-1 receptors leads to faster detachment (Fig. 9 *a*, *solid lines*). Increases in $f_{Nt}$ simultaneously reduce the steady-state peeling velocity, $\bar{V}_{pss}$, of the patch while increasing the peeling of non-patch regions (Fig. 9 *a*, *inset*). Enhanced clustering of receptors severely diminishes the density of adhesive cross-bridges in non-patch regions, but only modestly

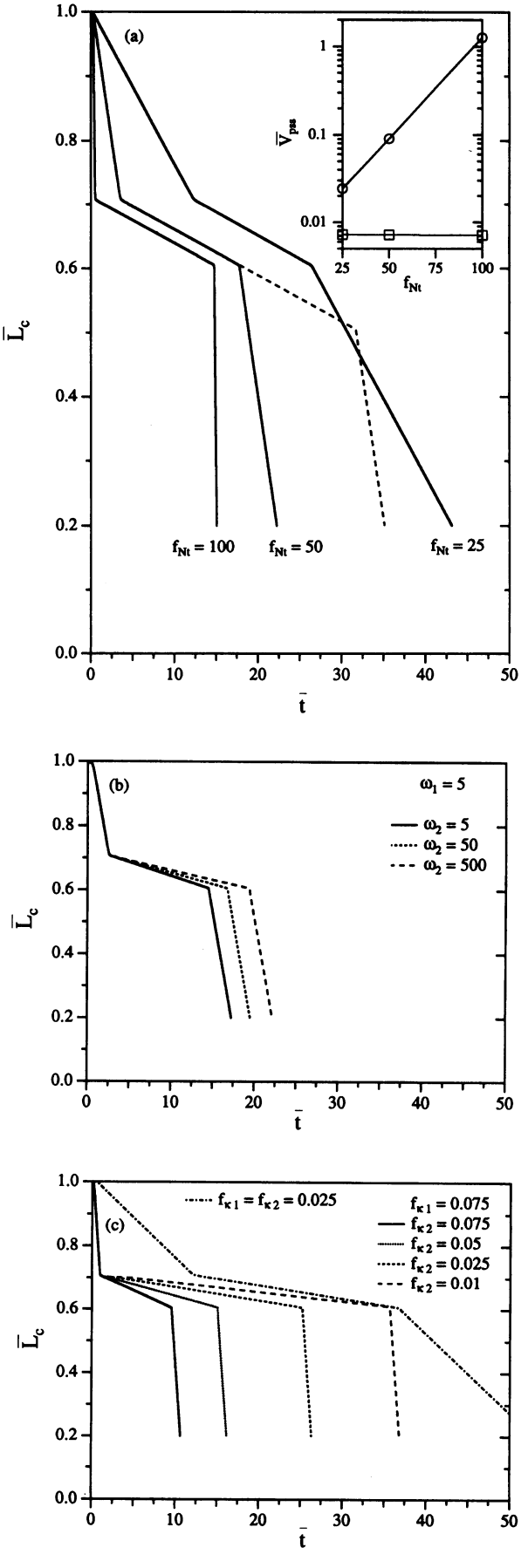


FIGURE 9 A qualitative comparison of our model to the experimental measurements of Tözeren et al. (1992) for the detachment of T lymphocytes from an ICAM-1 substrate. (*a–c*) The dimensionless contact radius data, $\bar{L}_c$, is plotted versus the nondimensional time, $\bar{t}$. (*a*) Greater receptor clustering (increases in $f_{Nt}$) results in faster membrane detachment (*solid line*) because the steady-state peeling velocity, $\bar{V}_{pss}$, of non-patch regions (*inset*, ○) is more strongly dependent on $f_{Nt}$ than is $\bar{V}_{pss}$ for the patch (*inset*, □). (*b*) For a constant level of affinity ($\omega_1$) between ligand and receptors located outside the patch, a substantial (100×) enhancement in the affinity ($\omega_2$) of clustered receptors for ligand only slightly delays detachment. (*c*) Effect of decreasing $f_{\kappa 2}$, or simultaneously decreasing $f_{\kappa 1}$ and $f_{\kappa 2}$ on detachment dynamics. Parameter values are $\alpha = 0.503$, $\beta_1 = \beta_2 = 48.8$, $\delta = 5 \times 10^{-3}$, $\delta_p = 0.1$, $\epsilon = 2$, $\zeta = 8000$, $\phi_1 = \phi_2 = 1.6 \times 10^5$, $\omega_1 = \omega_2 = 50$, $f_{\kappa 1} = f_{\kappa 2} = 0.05$, $f_{Nt} = 50$, $N_{bcrit} = 10^{-4}$, $P_{beg} = 0.3$, and $T_{mac} = 0.1$ dyn cm$^{-1}$, except where indicated.

supplements the bond density within patches because the maximum possible bond density is limited by available ligand ($\alpha\epsilon < 1$). During peeling, $\bar{V}_{pss}$ of the patch (*squares*) is much less sensitive to changes in $f_{Nt}$ than is the steady-state velocity of regions outside the patch (*circles*). The large difference in steady-state peeling velocities suggests that the detachment time is largely controlled by the length of the adhesive patch. Indeed, doubling the patch length when $f_{Nt} = 50$ increases the required time for cell detachment nearly twofold (*dashed line*).

Because activation of lymphocytes, either by cross-linking of the T-cell receptor on the lymphocyte surface or by phorbol ester (e.g., PMA) addition, induces a rapid enhancement in the affinity between LFA-1 receptors and ICAM-1 molecules (Dustin and Springer, 1989), we investigate how increases in affinity affect peeling when the amount of clustering is fixed ($f_{Nt} = 50$) in Fig. 9 *b*. In this figure, receptors outside the patch maintain a constant level of adhesiveness ($\omega_1 = 1$) while the avidity of clustered receptors ($\omega_2$) is increased. Although detachment requires more time as $\omega_2$ is raised, a 100-fold change in affinity has a relatively minor influence on the detachment kinetics.

In contrast to the effects of receptor-ligand affinity, increases in the strength (decreases in $f_{\kappa 2}$) of adhesive cross-bridges within the patch have a substantial impact on the total peeling time, $\bar{t}_p$ (Fig. 9 *c*). When the reactive compliance of bonds in non-patch regions equals that of bonds within the patch and is rather high ($f_{\kappa 1} = f_{\kappa 2} = 0.075$), $\bar{t}_p \approx 12.5$ (*solid line*). Much longer times ($\bar{t}_p > 50$) are necessary for detachment if the strength of all receptor-ligand cross-bridges is equally enhanced ($f_{\kappa 1} = f_{\kappa 2} = 0.025$). We also consider the possibility that bond strength is modulated solely by receptor-cytoskeleton association and, therefore, is limited to clustered bonds. This scenario is examined by decreasing $f_{\kappa 2}$ for fixed $f_{\kappa 1}$ (=0.075). In general, detachment occurs at later times as the strength of bonds within the patch is augmented. For example, although detachment occurs at $\bar{t} \approx 12.5$ when $f_{\kappa 2} = 0.075$, a threefold reduction in $f_{\kappa 2}$ (=0.025) extends the necessary time for detachment to $\bar{t}_p \approx 27.5$. Fig. 9 *c* clearly demonstrates that biochemical alterations of receptor-ligand bonds that alter the reactive compliance have a significant influence on the observed detachment kinetics.

Although the comparison between our model and the experimental measurements of T lymphocyte detachment from ICAM-1 substrates (Tözeren et al. 1992) was qualitative in nature, we can still draw some important conclusions from this analysis. First, our study shows that receptor clusters within the contact region peel substantially slower than other areas. Therefore, we find that cell detachment occurs through a combination of rapid and slow peeling, consistent with the general detachment behavior of T lymphocytes. This comparison also suggests that for the T lymphocyte/ICAM-1 system used by Tözeren et al. (1992), changes in the strength (i.e., reactive compliance) of receptor-ligand bonds have a much greater impact on the detachment dynamics than do alterations in the chemical affinity between receptors and ligand molecules. Finally, because we have assumed that the dissociation rate of unstressed bonds ($k_{req}$) equals 1 $s^{-1}$, the nondimensional time exactly corresponds to dimensional time. In this case, our model predicts detachment times (10–60 s) that are comparable with the reported times for T lymphocyte peeling (see Fig. 8).

## DISCUSSION

In this paper, we presented a theoretical framework that examines the influence of receptor clustering on cell detachment dynamics. Our model incorporates both the chemical kinetics of receptor-ligand bond formation and the mechanical response of the cell membrane to stresses to determine the rate at which the cell-substrate interface peels when receptors are clustered within discrete patches. Because aggregation of adhesion receptors into patches is an essential step in the development of specialized attachment structures such as focal and point contacts (Burridge et al., 1988; Tawil et al., 1993), this analysis should further our understanding of cellular modulation of adhesive behavior.

We demonstrated that receptor clusters (i.e., patches) substantially reduce the rate of cell detachment. Increases in the extent of receptor clustering, the ligand density, the receptor-ligand affinity, and the strength of cross-bridges (relative to the bending stiffness) were all found to diminish the steady-state peeling velocity of the patch. Interestingly, we found that the critical tension, based on a membrane of infinite extent, was not an appropriate measure of the strength of adhesion of a finite patch if the patch length, $\delta_p$, is less than the length over which membrane bending occurs, $\tau$. In such a case, the steady-state peeling velocity is not defined. When $\delta_p < \tau (\tau \approx 0.02)$, detachment of the patch is possible even when the applied tension equals the critical tension for an infinite patch of equivalent density, although the peeling velocity is nearly zero during peeling of the patch. This suggests that receptor clusters that are less than 0.2 $\mu$m in length (i.e., point contacts; see Streeter and Rees (1987) and Tawil et al. (1993)) may alter peeling kinetics by delaying, but not preventing, cell detachment. Because $T_{crit}$ for an infinite membrane is a valid description of the tension required to peel when $\delta_p \gg \tau$ (as is the case for focal contacts which are typically 2–10 $\mu$m in length), this finding validates our earlier steady-state analysis of the adhesive strength of focal contacts (Ward and Hammer, 1993).

Because LFA-1 receptors on PMA-treated lymphocytes may be clustered through cytoskeleton association after phorbol ester (e.g., PMA) addition (Burn et al., 1988), we performed a qualitative comparison between our model and recent experimental measurements (Tözeren et al., 1992) of the detachment of PMA-treated T lymphocytes from ICAM-1 substrates. The initial peeling of T lymphocytes was slow and preceded a much more rapid peeling of the membrane that continued until detachment was complete (Fig. 8) (Tözeren et al., 1992). Although the degree of receptor clustering on the lymphocyte surface was not ascertained by Tözeren and colleagues, we showed that the observed detachment behavior (i.e., intervals of slow and fast peeling)

can be explained by the presence of receptor clusters within the cell-substrate interface and found that the detachment time is strongly dependent on the reactive compliance of receptor-ligand cross-bridges (Fig. 9). These results suggest that through cytoskeletal reorganization, the T lymphocyte may dramatically modulate its adhesive behavior by simultaneously clustering receptors and decreasing the reactive compliance of bonds that form within these clusters. However, receptor clustering may represent only a single component affecting the detachment of T lymphocytes from ICAM-1 substrates; additional factors that may be important but were not considered in our comparison include a) changes in the bending rigidity of the membrane-cytoskeleton complex inside the adhesive patch, which would require the patch to fracture instead of peel (Ward and Hammer, 1993), b) active extension of cytoskeletal filaments, c) increased resistance to cell deformation (i.e., membrane bending) as detachment proceeds (Tözeren et al., 1992), and d) changes in the applied tension as the cell deforms during aspiration.

One limitation of our analysis is the absence of overall cell deformation during detachment. During a typical detachment experiment, the applied detachment force is transmitted to the cell-substrate contact through the cell membrane and cell body. If the cell-substrate attachment is very strong, as is the case within receptor clusters, substantial deformation of the cell may occur before and during detachment. Therefore, to determine more accurately the detachment behavior of cells forming receptor clusters, future analyses should consider how changes in cell geometry during detachment affect the transient and steady-state peeling of the membrane.

A second limitation concerns the numerical scheme we implement to calculate the peeling velocities of the adhesive patch. Because our finite difference algorithm uses explicit time-differencing, very small time steps and, thus, long computation times are required for numerical accuracy and stability (Appendix A), especially when the dimensionless forward rate constant, $k_f N_l$, becomes large (i.e., high ligand densities or affinities).

Although we have implicitly imbedded the action of cytoskeletal cross-linking molecules within the clustering factor, $f_{Nt}$, in this analysis, our future work will incorporate specific receptor-cytoskeleton linkages into this framework. We previously investigated how receptor-cytoskeleton patches affect cell-substrate attachment strength and found that the required detachment force depended greatly on the structural rigidity of the receptor-cytoskeleton plaque (Ward and Hammer, 1993). By adding cytoskeletal molecules that exert mechanical stresses on the cell membrane to the present model, we shall examine how the detachment kinetics are altered by increases in the rigidity of receptor-cytoskeleton or cytoskeleton-cytoskeleton connections within receptor clusters, and attempt to bridge the gap between the peeling and fracture modes of detachment described in our earlier work (Ward and Hammer, 1993).

This work was supported by a grant from the Cornell Biotechnology Program, which is sponsored by the New York State Science and Technology Foundation, a consortium of industries, the United States Army Research Office and the National Science Foundation, a National Science Foundation grant to Daniel A. Hammer (BCS-9009506), and a National Institutes of Health grant to Micah Dembo (R01AI21002-07).

## APPENDIX A

In this section, we present the nondimensional model equations governing the detachment kinetics of a membrane segment when adhesion receptors are clustered within discrete patches. We also describe the solution procedure and discuss the accuracy of the numerical method.

The dimensionless equations are obtained by defining the following scalings: $\bar{x} = x/L$; $\bar{y} = y/\lambda$; $\bar{s} = \bar{s}/L$; $\bar{C} = CL^2/\lambda$; $\bar{T} = TL^2/B$; $\bar{t} = tk_{req}$; $\bar{N}_b = N_b A_{cell}/R_l$; $\bar{N}_t = N_t A_{cell}/R_l$; $\bar{V}_p = V_p/k_{req}L$.

The equations of mechanical equilibrium for the membrane become

$$\frac{\partial^2 \bar{C}}{\partial \bar{s}^2} - \bar{C}\bar{T} = -\zeta\phi_i \bar{N}_b(\bar{y} - 1)\frac{\partial \bar{x}}{\partial \bar{s}} \tag{A1}$$

and

$$\frac{\partial \bar{T}}{\partial \bar{s}} + \left(\frac{\delta^2}{2}\right)\frac{\partial \bar{C}^2}{\partial \bar{s}} = \delta^2\zeta\phi_i \bar{N}_b(\bar{y} - 1)\frac{\partial \bar{y}}{\partial \bar{s}}, \tag{A2}$$

where we use the subscript $i$ to distinguish between the properties of receptors that are clustered within the adhesive patch ($i = 2$) and those that are located outside the patch ($i = 1$).

The dimensionless arclength and curvature expressions are

$$\left(\frac{\partial \bar{x}}{\partial \bar{s}}\right)^2 + \delta^2\left(\frac{\partial \bar{y}}{\partial \bar{s}}\right)^2 = 1 \tag{A3}$$

and

$$\bar{C} = \left(\frac{\partial \bar{x}}{\partial \bar{s}}\right)\left(\frac{\partial^2 \bar{y}}{\partial \bar{s}^2}\right) - \left(\frac{\partial^2 \bar{x}}{\partial \bar{s}^2}\right)\left(\frac{\partial \bar{y}}{\partial \bar{s}}\right). \tag{A4}$$

In the cell reference frame, the bond density at any membrane position within the cell-substrate interface is obtained from solution of the nondimensional continuity equation,

$$\frac{\partial \bar{N}_b}{\partial \bar{t}} = \bar{V}_p\frac{\partial \bar{N}_b}{\partial \bar{s}} + \omega_i \bar{k}_r \bar{K}(\epsilon - \bar{N}_b)(\bar{N}_t - \bar{N}_b) - \bar{k}_r \bar{N}_b, \tag{A5}$$

where $\bar{k}_r = \exp\{\beta_i f_{xi}(\bar{y} - 1)^2\}$ and $\bar{K} = \exp\{-\beta_i(\bar{y} - 1)^2\}$. Convection of the adhesive patch is measured by the time-dependent change in the total receptor density,

$$\frac{\partial \bar{N}_t}{\partial \bar{t}} = \bar{V}_p\frac{\partial \bar{N}_t}{\partial \bar{s}}. \tag{A6}$$

The solution to Eqs. A1–A6 must satisfy certain boundary and matching conditions (Evans, 1985a, b; Dembo et al., 1988; Ward and Hammer, 1993). Because the membrane is firmly clamped to the substrate at the center of contact, $\bar{y} = 1$ and $(\partial \bar{y}/\partial \bar{s}) = 0$ at $\bar{s} = 1$. At the contact point ($\bar{s} = 0$), the bond density, $\bar{N}_b$, equals a critical value, $N_{bcrit}$, to ensure that membrane stresses are negligible at this point. Partial integration of the equations of membrane mechanical equilibrium within the macroscopic region (where $\bar{N}_b = 0$) yields matching conditions that relate the membrane tension, curvature, and transverse shear at $\bar{s} = 0$ to the macroscopic tension, $\bar{T}_{mac}$, curvature, $\bar{C}_{mac}$, and contact angle, $\theta_{mac}$, (Evans, 1985a, b; Dembo et al., 1988),

$$\bar{T} = \bar{T}_{mac}\cos(\theta_{mac} - \theta_{mic}), \tag{A7}$$

$$(\bar{C})^2 = (\bar{C}_{mac})^2 + (2\bar{T}_{mac}/\delta^2)[1 - \cos(\theta_{mac} - \theta_{mic})], \tag{A8}$$

and

$$\frac{\partial \bar{C}_{mic}}{\partial \bar{s}} = \left(\frac{\bar{T}_{mac}}{\delta}\right)\sin(\theta_{mac} - \theta_{mic}). \tag{A9}$$

Solution of this nonlinear system of equations (A1–A9) yields the cell-substrate separation, bond density, and tension as functions of membrane position. The peeling velocity is calculated from Eq. A5, evaluated at the contact point. The microscopic membrane region is divided into a one-dimensional grid with a finer mesh-size employed near the edge of contact because membrane bending is greatest in this region. The iterative procedure is begun by providing an initial estimate for the bond density distribution: $N_b = 0$ for $\bar{s} < 0$, $N_b = N_{bc}$ for $\bar{s} = 0$, and $N_b = N_{beqi}$ for $\bar{s} > 0$ ($i = 1$, outside patch; $i = 2$ inside patch). Next, the discretized forms of the curvature relation (A4) and the matching conditions on curvature (A8) and transverse shear (A9) are substituted into the normal force balance equation (A1). For fixed tension, $x$ coordinates, and bond density, the resulting banded matrix is solved to determine the cell-substrate separation subject to the appropriate boundary conditions. The arclength expression (A3) is used to update the $x$ coordinates, whereas the membrane tension is determined from numerical integration of Eq. A2. The bond balance (Eq. A5) is solved for the bond density distribution. Within each time step, this cycle is repeated until the membrane morphology converges. When this occurs, the new peeling velocity is calculated and the time is incremented.

An additional step is required to deal with a patch. Because of numerical diffusion, the initial sharp discontinuities in receptor density, $\bar{N}_t$, and bond density, $\bar{N}_b$, at the patch boundary become spread over a number of grid points. This behavior results from numerical inaccuracies in accounting for the convection of the patch in the cell reference frame. The first order upwind transport scheme (Dembo et al., 1988) used when $\bar{N}_t$ and $\bar{N}_b$ are uniform is no longer adequate. Instead, we implement a monotonic transport scheme (van Leer, 1977; Hawley et al., 1984) and find that numerical diffusion is limited to a few grid points in this case. However, this scheme requires explicit time differencing, which presents additional problems (see below).

Several tests were used to determine the accuracy of our numerical methodology. In the absence of receptor clustering and ligand depletion, we calculated $\bar{V}_p$ ($\bar{t}$) for parameter sets examined by Dembo and colleagues (1988). In all cases, our model results were identical to the published data. The algorithm also gave the correct tension at the center of contact ($\bar{T} = 0$ at $\bar{s} = 1$ because $\theta_{mac} = 90°$) and at the macroscopic edge (integration of Eq. A2 yields $\bar{T} = \bar{T}_{mac}$). When ligand depletion was incorporated into our model, these numerical checks on membrane tension were still satisfied, the steady-state peeling velocity, $\bar{V}_{pss}$, was identically zero when $\bar{T}_{mac} = \bar{T}_{crit}$, and at high ligand densities (i.e., ligand depletion is negligible), $\bar{V}_{pss}$ followed the analytic expression derived by Dembo et al. (1988). These same tests were performed on the algorithm used to determine the peeling velocity of a receptor cluster. In all cases, numerical accuracy and stability were achieved provided the time step satisfied the Courant condition, $\Delta\bar{t} \leq \Delta\bar{s}/\bar{V}_p$, where $\Delta\bar{s}$ is the grid spacing, and was not large compared with the binding reactions ($k_f N_l)^{-1}$ or $k_r^{-1}$) in the vicinity of $\bar{s} = 0$. At high ligand densities and affinities, this condition necessitated using a much smaller time step than needed in the implicit method, thereby making computation of $\bar{V}_{pss}$ quite lengthy.

## REFERENCES


Akiyama, S. K., K. Nagata, and K. M. Yamada. 1990. Cell surface receptors for extracellular matrix components. *Biochim. Biophys. Acta.* 1031: 91–110.

Bell, G. I. 1978. Models for the specific adhesion of cells to cells. *Science.* 200:618–627.

Bell, G. I., M. Dembo, and P. Bongrand. 1984. Cell adhesion: competition between nonspecific repulsion and specific bonding. *Biophys. J.* 45:1051–1064.

Ben-Ze'ev, A., G. S. Robinson, N. L. Bucher, and S. R. Farmer. 1988. Cell-cell and cell-matrix interactions differentially regulate the expression of hepatic and cytoskeletal genes in primary cultures of rat hepatocytes. *Proc. Natl. Acad. Sci. USA.* 85:2161–2165.

Burn, P., A. Kupfer, and S. J. Singer. 1988. Dynamic membrane-cytoskeletal interactions: Specific association of integrin and talin arises in vivo after phorbol ester treatment of peripheral blood lymphocytes. *Proc. Natl. Acad. Sci. USA.* 85:497–501.

Burridge, K., K. Fath, T. Kelly, G. Nuckolls, and C. Turner. 1988. Focal adhesions: transmembrane junctions between the extracellular matrix and the cytoskeleton. *Ann. Rev. Cell Biol.* 4:487–525.

Couchman, J. R., and D. A. Rees. 1979. The behaviour of fibroblasts migrating from chick heart explants: Changes in adhesion, locomotion and growth, and in the distribution of actomyosin and fibronectin. *J. Cell Sci.* 39:149–165.

Cozens-Roberts, C., J. A. Quinn, and D. A. Lauffenburger. 1990. Receptor-mediated adhesion phenomena. Model studies with the radial-flow detachment assay. *Biophys. J.* 58:107–125.

Dejana, E., S. Colella, G. Conforti, M. Abbadini, M. Gaboli, and P. C. Marchisio. 1988. Fibronectin and vitronectin regulate the organization of their respective Arg-Gly-Asp adhesion receptors in cultured human endothelial cells. *J. Cell Biol.* 107:1215–1223.

Dembo, M., D. C. Torney, K. Saxman, and D. Hammer. 1988. The reaction-limited kinetics of membrane-to-surface adhesion and detachment. *Proc. R. Soc. Lond. B.* 234:55–83.

Dustin, M. L., and T. A. Springer. 1989. T-cell receptor cross-linking transiently stimulates adhesiveness through LFA-1. *Nature.* 341:619–624.

Duwe, H. P., J. Kaes, and E. Sackmann. 1990. Bending elastic moduli of lipid bilayers: Modulation by solutes. *J. Phys. France.* 51:945–962.

Engelhardt, H., H. P. Duwe, and E. Sackmann. 1985. Bilayer bending elasticity measured by Fourier analysis of thermally excited surface undulations of flaccid vesicles. *J. Physique Lett.* 46:395–400.

Evans, E. A. 1983. Bending elastic modulus of red blood cell membrane derived from buckling instability in micropipet aspiration tests. *Biophys. J.* 43:27–30.

Evans, E. A. 1985a. Detailed mechanics of membrane-membrane adhesion and separation. I. Continuum of molecular cross-bridges. *Biophys. J.* 48: 175–183.

Evans, E. A. 1985b. Detailed mechanics of membrane-membrane adhesion and separation. II. Discrete kinetically trapped molecular cross-bridges. *Biophys. J.* 48:185–192.

Evans, E. A., and R. Skalak. 1980. Mechanics and Thermodynamics of Biomembranes. CRC Press, Boca Raton, FL. 254 pp.

Fath, K. R., C.-J. Edgell, and K. Burridge. 1989. The distribution of distinct integrins in focal contacts is determined by the substratum composition. *J. Cell Sci.* 92:67–75.

Hammer, D. A., and S. M. Apte. 1992. Simulation of cell rolling and a hesion on surfaces in shear flow: general results and analysis of selectin-mediated neutrophil adhesion. *Biophys. J.* 63:35–57.

Hawley, J. F., L. L. Smarr, and J. R. Wilson. 1984. A numerical study of nonspherical black hole accretion. II. Finite differencing and code calibration. *Astrophys. J. Suppl. Series.* 55:211–246.

Ingber, D. E. 1990. Fibronectin controls capillary endothelial cell growth by modulating cell shape. *Proc. Natl. Acad. Sci. USA.* 87:3579–3583.

Ingber, D. E., and J. Folkman. 1989. Mechanochemical switching between growth and differentiation during fibroblast growth factor-stimulated angiogenesis *in vitro*: role of extracellular matrix. *J. Cell Biol.* 109:317–330.

Izzard, C. S., and L. R. Lochner. 1976. Cell-to-substrate contacts in living fibroblasts: an interference-reflexion study with an evaluation of the technique. *J. Cell Sci.* 21:129–159.

Lotz, M. M., C. A. Burdsal, H. P. Erickson, and D. R. McClay. 1989. Cell adhesion to fibronectin and tenascin: quantitative measurements of initial binding and subsequent strengthening response. *J. Cell Biol.* 109: 1795–1805.

Marcantonio, E. E., J.-L. Guan, J. E. Trevithick, and R. O. Hynes. 1990. Mapping of the functional determinants of the integrin $\beta_1$ cytoplasmic domain by site-directed mutagenesis. *Cell Regulation.* 1:597–604.

Massia, S. P., and J. A. Hubbell. 1990. Covalent surface immobilization of Arg-Gly-Asp- and Tyr-Ile-Gly-Ser-Arg-containing peptides to obtain well-defined cell-adhesive surfaces. *Anal. Biochem.* 187:292–301.

Massia, S. P., and J. A. Hubbell. 1991. An RGD spacing of 440 nm is sufficient for integrin $\alpha_v\beta_3$-mediated fibroblast spreading and 140 nm for focal contact and stress fiber formation. *J. Cell Biol.* 114:1089–1100.

Mooney, D., L. Hansen, J. Vacanti, R. Langer, S. Farmer, and D. Ingber. 1992. Switching from differentiation to growth in hepatocytes: control by extracellular matrix. *J. Cell. Physiol.* 151:497–505.

Pecht, I., and D. Lancet. 1977. Kinetics of antibody-hapten interactions. *Mol. Biol. Biochem. Biophys.* 24:306–338.

Rees, D. A., C. W. Lloyd, and D. Thom. 1977. Control of grip and stick in cell adhesion through lateral relationships of membrane glycoproteins. *Nature.* 267:124–128.

Reszka, A. A., Y. Hayashi, and A. F. Horwitz. 1992. Identification of amino acid sequences in the integrin $\beta_1$ cytoplasmic domain implicated in cytoskeletal association. *J. Cell Biol.* 117:1321–1330.

Roitt, I., J. Brostoff, and D. Male. 1989. Immunology. Gower Medical Publishing, London. 325 pp.

Springer, T. A. 1990. Adhesion receptors of the immune system. *Nature.* 346:425–434.

Streeter, H., and D. Rees. 1987. Fibroblast adhesion to RGDS shows novel features compared with fibronectin. *J. Cell Biol.* 105:507–515.

Sung, K.-L. P., P. Kuhlman, F. Maldonado, B. A. Lollo, S. Chien, and A. A. Brian. 1992. Force contribution of the LFA-1/ICAM-1 complex to T cell adhesion. *J. Cell Sci.* 103:259–266.

Tawil, N., P. Wilson, and S. Carbonetto. 1993. Integrins in point contacts mediate cell spreading: factors that regulate integrin accumulation in point contacts vs. focal contacts. *J. Cell Biol.* 120:261–271.

Tözeren, A. 1989. Adhesion induced by mobile cross-bridges: steady state peeling of conjugated pairs. *J. Theor. Biol.* 140:1–17.

Tözeren, A., K.-L. Sung, L. A. Sung, M. L. Dustin, P.-Y. Chan, T. A. Springer, and S. Chien. 1992. Micromanipulation of adhesion of a Jurkat cell to a planar bilayer membrane containing lymphocyte function-associated antigen 3 molecules. *J. Cell Biol.* 116:997–1006.

van Leer, B. 1977. Towards the ultimate conservative difference scheme. IV. A new approach to numerical convection. *J. Comput. Phys.* 23: 276–299.

Ward, M. D., and D. A. Hammer. 1993. A theoretical analysis for the effect of focal contact formation on cell-substrate attachment strength. *Biophys. J.* 64:936–959.

Watt, F. M., P. W. Jordan, and C. H. O'Neill. 1988. Cell shape controls terminal differentiation of human epidermal keratinocytes. *Proc. Natl. Acad. Sci. USA.* 85:5576–5580.